Biosensors and Bioelectronics 168 (2020) 112508

Contents lists available at ScienceDirect

Biosensors and Bioelectronics

journal homepage: http://www.elsevier.com/locate/bios

Refractive index tuning of SiO_2 for Long Range Surface Plasmon Resonance based biosensor

Surbhi Jain [a], Ayushi Paliwal [a], Vinay Gupta [a], Monika Tomar [b,*]

[a] Department of Physics and Astrophysics, University of Delhi, Delhi, 110007, India
[b] Department of Physics, Miranda House, University of Delhi, Delhi, 110007, India

ARTICLE INFO

Keywords:
LRSPR
SiO_2
Nanostructures
Biosensor
Refractive index tuning
Uric acid

ABSTRACT

A novel, highly sensitive and low cost Long Range Surface Plasmon Resonance (LRSPR) biosensor for detecting uric acid, as a model analyte, has been developed in this work. Silicon dioxide (SiO_2) having low and tunable refractive index has been chosen as the dielectric layer for the excitation of LRSP modes replacing the most explored Cytop and Teflon polymers. The prepared LRSPR based uric acid bio-sensor gives good response characteristics with a high sensitivity of about 21.6°/mM and low limit of detection (LOD) of 0.02 mM. The fabricated LRSPR sensor was also evaluated to detect uric acid in real serum samples. The results yield a great scope to promote the development of robust, efficient and highly selective LRSPR based biosensors with SiO_2 as tunable dielectric layer.

1. Introduction

Over the period of time, optical sensors have made their way into commercial market due to numerous advantages such as completely passive, ability to be used in explosive environment, immunity to Electromagnetic interference, high biocompatibility, non-intrusive nature and remote operation (Ahuja and Parande, 2012; Colette McDonagh et al., 2008). Surface plasmon resonance (SPR) is believed to be one of the most reliable and sensitive technique amongst various available optical techniques (Damborsky et al., 2016) and has gained much attention amongst the research community for the development of various sensors (Manera and Rella, 2013; Nooke et al., 2010). However, the conventional SPR sensors suffer from relatively low sensitivity and large full width at half maxima (FWHM), which plays an important factor when the analyte under study such as bio-entities have size comparable to or larger than the penetration depth of the surface plasmons (Dostálek et al., 2007). The low penetration depth of SPR imposes a constraint on the response range and also distorts the reflected signal (Alastair W. Wark et al., 2005). The large FWHM accounts for the relatively low sensitivity and poor precision of the SPR based sensor leading to low signal to noise ratio (Yuan and Dai, 2014). To overcome these limitations, Long Range Surface Plasmon Resonance (LRSPR) can be utilized (Berini, 2009).

Symmetric and Anti-Symmetric: Two guided Plasmon wave modes are originated by a metal layer embedded between the two identical dielectric medium of same refractive index (Dielectric-Metal-Dielectric) in a symmetric configuration (Krupin et al., 2015). Symmetric mode acknowledged as Long Range Surface Plasmon (LRSP) mode is the one which posses a symmetrical profile of the electromagnetic field with respect to the center of metal layer and it arises because of the constructive interference between the two Surface Plasmon Waves (SPWs) generated at the two metal-dielectric interfaces (Berini, 2009). On the other side, Anti-Symmetric mode possesses an anti-symmetric field profile which is formed as a result of the destructive interference between the two SPWs and is comparatively less sensitive to any change in its ambience as compared to the symmetric mode (Berini, 2009). Refractive index matching of two dielectric media is an essential aspect for the generation of the LRSP mode. LRSPs can traverse along the metal thin film with an order of magnitude higher than the conventional surface plasmons (Berini et al., 2007). Thus, the LRSPs excitation is mainly acknowledged with a narrower width of resonance dip and enhanced electromagnetic field intensity, making it a potential candidate for biosensing applications (Kasry and Knoll, 2006). LRSPR is explored extensively for quantifying the change in refractive index caused due to target biomolecules (analyte) binding, present in an aqueous sample with the specific recognition sites of the biomolecules (bioreceptor) immobilized on the metal layer (Dostálek et al., 2007). Due to lower damping characteristics, LRSPs facilitate measurement of

* Corresponding author.
E-mail address: monikatomar@gmail.com (M. Tomar).

https://doi.org/10.1016/j.bios.2020.112508
Received 30 April 2020; Received in revised form 23 July 2020; Accepted 9 August 2020
Available online 20 August 2020

very minute variations in the refractive index (Slavík and Homola, 2007) and thus enable accurate detection of biomolecular binding events in comparison to the conventional SPR biosensors (A W Wark et al., 2005).

Most of the work reported on LRSPR based biosensors utilize polymers such as Teflon and Cytop as the dielectrics for the excitation of LRSP mode as they have refractive index values of 1.31 and 1.33 respectively, which are almost similar to the refractive index of water (~1.33) (Béland et al., 2015; Méjard et al., 2013). However, thin films of these polymers can be prepared only by chemical route, which posses inhomogeneous film quality with lots of defects and are difficult to reproduce (Wang et al., 2009). Also these polymers cannot withstand elevated temperatures and are more expensive (Paliwal et al., 2018). Therefore researchers have been trying hard to come up with alternative inorganic materials and one promising material is Silicon Dioxide (SiO_2). SiO_2 is wide energy band gap material making it able to work at high temperatures and in harsh environmental conditions (Deshmukh

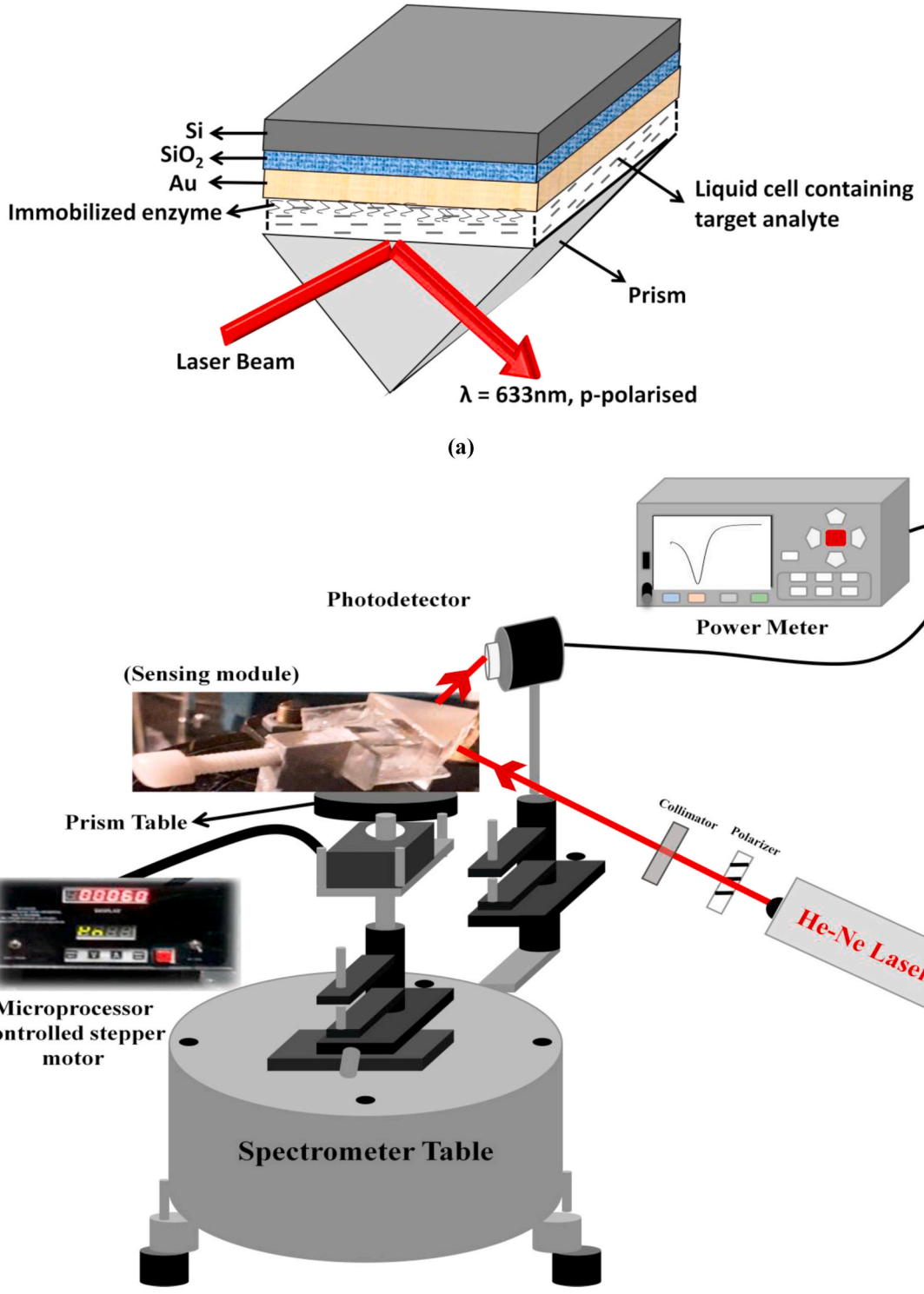

Fig. 1. Schematic of the (a) Proposed sensor structure Prism/Analyte/Enzyme/SiO_2/Si, and (b) Complete LRSPR sensor set up.

and Aydil, 1994). It is chemically very stable, non-reactive and bio-compatible (Astrova and Tolmachev, 2000). However, the reported value of refractive index (n) of bulk SiO_2 is 1.49 (Matsuoka et al., 1991). Refractive index of SiO_2 thin film can be lowered to match with the refractive index of water (~1.33), by depositing its nanostructures owing to the fact that the feature size of nanostructures are less as compared to the wavelength of incident visible light thereby reducing the Rayleigh and Mie scattering (Xi et al., 2007). The reduction in both these scatterings leads to increased transmission of the incident visible light and hence the effective refractive index is low. The nanostructured SiO_2 films, with high porosity and low refractive index, can be grown by oblique-angle deposition technique (Astrova and Tolmachev, 2000). Hence, in the present work SiO_2 nanostructured films with tunable refractive index are grown by oblique-angle RF sputtering technique and further exploited as the dielectric layer for the development of LRSPR based biosensor. As far as our knowledge goes, no report is available in literature on the development of LRSPR based biosensors utilizing SiO_2 as the dielectric layer.

Uric acid has been chosen as the model analyte in the present work for the fabrication of LRSPR biosensor. The excess or deficiency of uric acid in human blood and urine leads to various diseases like metabolic acidosis, lead poisoning, diabetes, leukemia, gout, swelling of the limbs, etc (Arora et al., 2014). To prevent these diseases, it is essential to keep a check on the uric acid levels in the human body to ensure that they are in normal physiological range.

The present work reports the development of a LRSPR based biosensor utilizing nanostructured SiO_2 thin film as the dielectric sensing layer, for detecting uric acid in the concentration range from 0.05 mM–1 mM. The schematics of the proposed LRSPR based biosensor structure and the devised sensor setups are shown in Fig. 1.

2. Experimental section

2.1. Optimization of SiO_2 thin film using RF sputtering

Nanostructured SiO_2 films are grown on Si substrate using RF sputtering technique in oblique angle configuration using a SiO_2 ceramic target (99.99% pure) under 100% Ar gas atmosphere at two different pressures of 20 mTorr and 30 mTorr. Two oblique angles i.e. 70° and 80° were chosen at each pressure. The growth conditions utilized for the deposition of SiO_2 nanostructured film are tabulated in Supplementary Table S1. The deposited SiO_2 films observed to be quite stable over a period of at least 24 weeks and are also anticipated to be stable at high operating temperatures up to 900 °C. The thickness of SiO_2 nanostructured film was ascertained by a surface profiler (Dektak 150, Veeco) and is kept fixed at 200 nm.

2.2. Characterization studies

Fourier-transform infrared (FTIR) Spectroscopy, Scanning electron microscope (SEM) and Atomic Force Microscope (AFM) are utilized to study the optical and morphological properties respectively of grown SiO_2 nanostructured films, details of which are mentioned in Supplementary file. SPR and Ellipsometry studies are employed for measurements of refractive index of the grown SiO_2 nanostructured films.

3. Results and discussion

3.1. Surface plasmon resonance (SPR)

SPR reflectance curves for the prism/air-gap/Au/SiO_2/Si system having SiO_2 nanostructured films grown under varying deposition

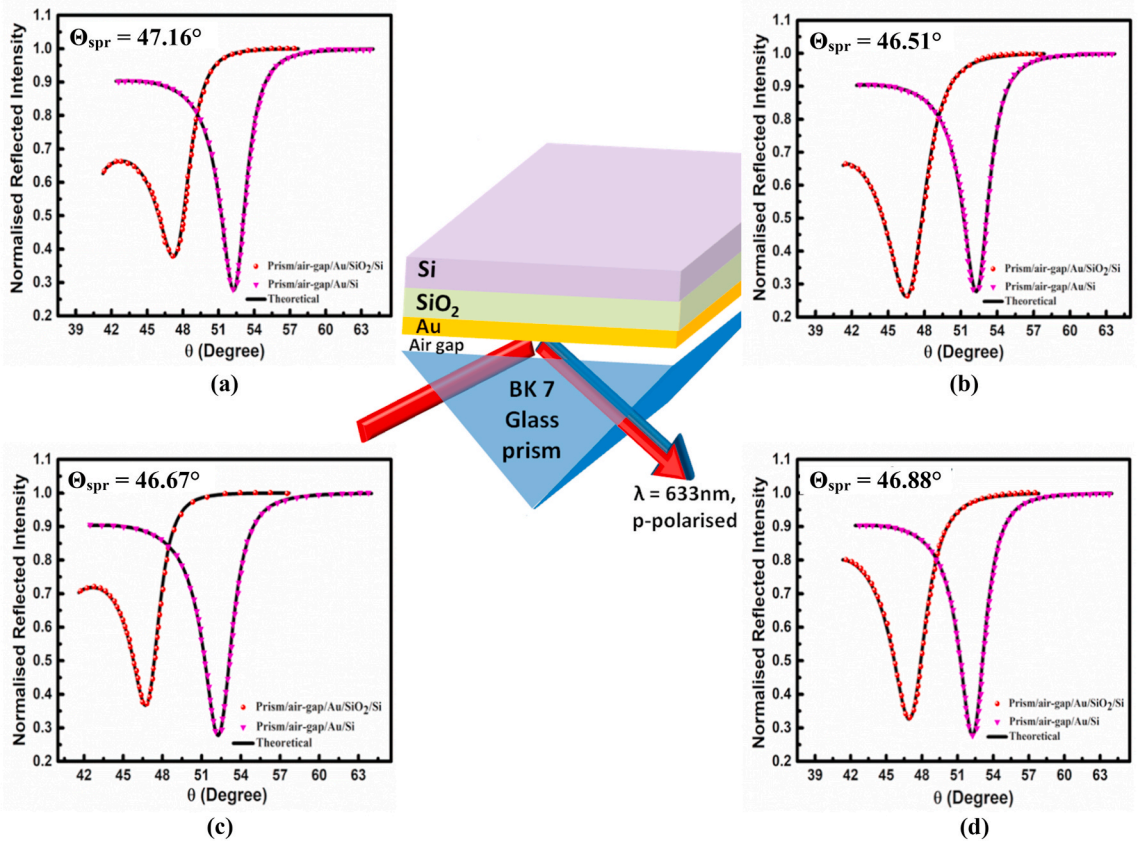

Fig. 2. Schematic of Otto configuration (centre) and SPR curves for Prism/air-gap/Au/SiO_2/Si structures consisting of SiO_2 thin film deposited at (a) 70° Oblique angle, 20 mTorr, (b) 70° Oblique angle, 30 mTorr, (c)80° Oblique angle, 20 mTorr, and (d) 80° Oblique angle, 30 mTorr.

conditions are shown in Fig. 2(a–d), where the symbols depicts the experimental data points and the solid constant line shows the corresponding theoretically fitted curves.. The representation of the Otto configuration setup utilized for the SPR measurements is shown in Fig. 2, details of which are mentioned in our previous work (Paliwal et al., 2018). SPR reflectance curves acquired for the prism/air-gap/Au/Si structure (without SiO_2 film) is also included in Fig. 2(a–d) for comparison. All the SPR reflectance curves show reduction in the reflected intensity with increment in the incident angle, attaining a minimum (dip) at SPR resonance angle (θ_{spr}) and afterwards begin increasing sharply with further enhancement in the incident angle (Fig. 2). It may be seen that the SPR reflectance curves (Fig. 2(a–d)) of all prepared prism/air-gap/Au/SiO_2/Si systems show a shift in the resonance angle (θ_{spr}) towards right i.e. at higher angle in comparison to the one obtained for the bare prism/air-gap/Au/Si system. This shift is accredited to the modification in dielectric media in the vicinity of Au layer from Si for prism/air-gap/Au/Si to SiO_2/Si for prism/air-gap/Au/SiO_2/Si structure. Further, different values of θ_{spr} and R_{min} are observed for the different prism/air-gap/Au/SiO_2/Si structures (Fig. 2 (a–d). This is assigned to modification in material property (refractive index) of SiO_2 film as the growth conditions are varied. Fresnel's equations are employed to estimate the refractive index (n) of the SiO_2 films deposited under varying deposition conditions (Dewan et al., 2018) and are listed in Supplementary Table S2. It is imperative to see that the values of refractive index of all grown SiO_2 nanostructured films are found to be lower than that reported for bulk SiO_2 (1.49). Amongst the four deposited SiO_2 films, the film deposited at 80° oblique angle and 30 mTorr pressure is found to possess lowest value of refractive index of 1.332 (Supplementary Table S2). As evident from FESEM image (Supplementary Fig. S2 (d)), SiO_2 film deposited at 80° oblique angle and 30 mTorr pressure posses maximum porous morphology, which supports the claim of obtained lowest refractive index (Xi et al., 2007).

3.2. Ellipsometry

Ellipsometry study was also performed on deposited SiO_2 nanostructured film using an Ellipsometer (Make: SEN research SE 850 DUV), to confirm the values of refractive index obtained from SPR measurement. The obtained refractive index values are listed in Supplementary Table S2 for comparison. The refractive index values obtained from Ellipsometry studies match very well with those obtained with SPR (Supplementary Table S2). Both Ellipsometry and SPR studies confirm that lowest refractive index (~1.33) is achieved for the SiO_2 nanostructured film deposited at 30 mTorr pressure and 80° oblique angle, which is further utilized as dielectric layer in the fabrication of LRSPR based uric acid biosensor.

3.3. LRSPR bio-sensing characteristics

The LRSPR based uric acid biosensor is realized using SiO_2 (deposited at 30 mTorr and 80° oblique angle) as the first dielectric layer over which Au layer of thickness 20 nm is coated using thermal evaporation technique. On top of the Au layer, 1 mM enzyme (Uricase) is immobilized to detect the presence of uric acid in its assay. To ensure the successful immobilization of uricase enzyme on the gold surface, FTIR spectra in the range 400–4000 cm^{-1}, has been acquired for the uricase/Au/SiO_2/Si structure and is shown in Supplementary Fig. S4. The sharp absorption bands obtained at 471 cm^{-1}, 852 cm^{-1} and 1001 cm^{-1} correspond to the characteristic SiO_2 film underneath the immobilized uricase enzyme. These bands are a little shifted with respect to the corresponding bands obtained for the bare SiO_2/Si structures (Supplementary Fig. S1), which may be accredited to the slight variation in the quantity of chemical species after the physical adsorption of the enzyme (Ryu et al., 2010). The sharp band observed at 1241 cm^{-1} is due to the stretching of C–N amine group (Jindal et al., 2017). The other intense absorption peaks are obtained at 1602 cm^{-1}, 2386 cm^{-1}, 2876 cm^{-1} and 3145 cm^{-1}which correspond to C═O stretching of primary amide group, stretching vibration of hydroxyl group, C–H stretches of alkyl and alkenyl group (Jindal et al., 2013) and stretching of N═H amide group respectively (Herrasti et al., 2016). Thus, it can be concluded from the FTIR spectrum of uricase/Au/SiO_2/Si structure that stretching frequencies corresponding to the amide groups are present, confirming successful immobilization of uricase on the surface of Au/SiO_2/Si surface.

A flow process of the steps followed in the fabrication of the proposed LRSPR biosensor is shown in Fig. 3. The uric acid (liquid analyte) is held in contact with uricase/Au/SiO_2/Si structure which acts as the second dielectric layer in the symmetrical dielectric-metal-dielectric configuration of LRSPR such that the requirement of refractive index matching between uric acid (~1.33) and SiO_2 (~1.33) has been fulfilled. The Long Range Surface Plasmons (LRSPs) in the dielectric (SiO_2)-Metal (Au)–Dielectric (Uricase-Uric acid) configuration were excited by a p-polarized He–Ne Laser ($\lambda = 633$ nm). The surface Plasmons excited at the two metal-dielectric interfaces couple constructively to form long range surface Plasmons. The laser was made to incident onto the prism/uric acid-uricase/Au/SiO_2/Si sensor configuration through one end of the prism as shown in Fig. 1(a) and (b). The sensor structure is placed on a prism table equipped with a micro controlled stepper motor (Fig. 1(b)). The reflected intensity of light from the other phase of the prism is measured with respect to the incident angle of laser light using a silicon photo-detector (Fig. 1(b)). The biosensing response characteristics of the prepared LRSPR sensor structure (prism/uric acid-uricase/Au/SiO_2/Si) were noted for a broad concentration range of Uric acid (0.05 mM–1 mM) separately as shown in Fig. 4 (a). The slight broadness in the LRSPR curves may be attributed to the losses associated with the damping of the incident light because of the scattering in the liquid analyte (uric acid) medium as well as the porosity of the deposited SiO_2 nanostructured films.

For reference, a buffer solution of Phosphate Buffer Saline (PBS) is filled in the liquid cell and the reference LRSPR reflectance curve for the Prism/PBS-uricase/Au/SiO_2/Si configuration has been taken (Fig. 4 (a)). The solutions of several concentrations of uric acid were put in the liquid cell separately and the reflected intensity for each concentration of uric acid is noted down as a function of incident angle (Fig. 4 (a)). After each measurement, the liquid cell is washed with buffer solution. As the uric acid concentration is increased from NIL (base PBS solution) to 1 mM, an incessant shift in the LRSPR reflectance curves towards lower angle is perceived (Fig. 4 (a)). When the LRSPs propagate along the two metal – dielectric interfaces (uric acid-uricase/Au and Au/SiO_2), any change in the second dielectric (Uric acid-uricase) will lead to a change in the electromagnetic field associated with the LRSPs, thereby resulting in a change in the propagation constant of LRSP wave. This leads to variation in the resonance conditions of interacting LRSPs and hence resulting in a shift in the resonance angle (Fig. 4 (a)). The variation in resonance angle of the LRSPR curves depend on the modification in dielectric constant (or refractive index) of the dielectric layer (uric acid-uricase) present in Prism/uric acid–uricase/Au/SiO_2/Si sensor system as per the Fresnel's equations discussed in the following section (Paliwal et al., 2014).

The reflectance for the five layered system (Prism/Uric acid-Uricase/Au/SiO_2/Si) at an incident angle θ is given as (Paliwal et al., 2018):

$$R_{12345} = \left| \frac{r_{12} + r_{2345} * f_2}{1 + r_{12} * r_{2345} * f_2} \right|^2 \quad (1)$$

$$r_{ik} = \frac{\left(\frac{k_{zi}}{\varepsilon_i} - \frac{k_{zk}}{\varepsilon_k} \right)}{\left(\frac{k_{zi}}{\varepsilon_i} + \frac{k_{zk}}{\varepsilon_k} \right)} \quad (2)$$

$$k_{zi} = \frac{2\pi}{\lambda} \left(\varepsilon_i - \varepsilon_1 \sin^2 \theta \right)^{\frac{1}{2}} \quad (3)$$

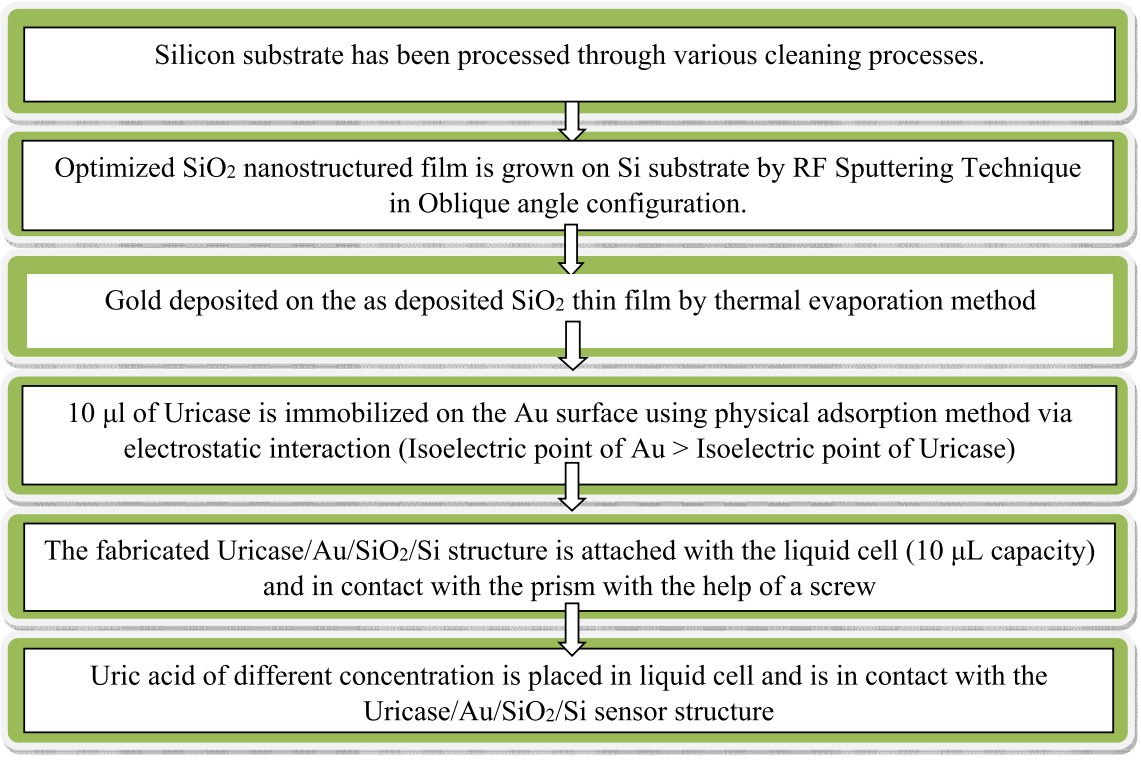

Fig. 3. Flow process of steps engaged in the fabrication of LRSPR biosensor.

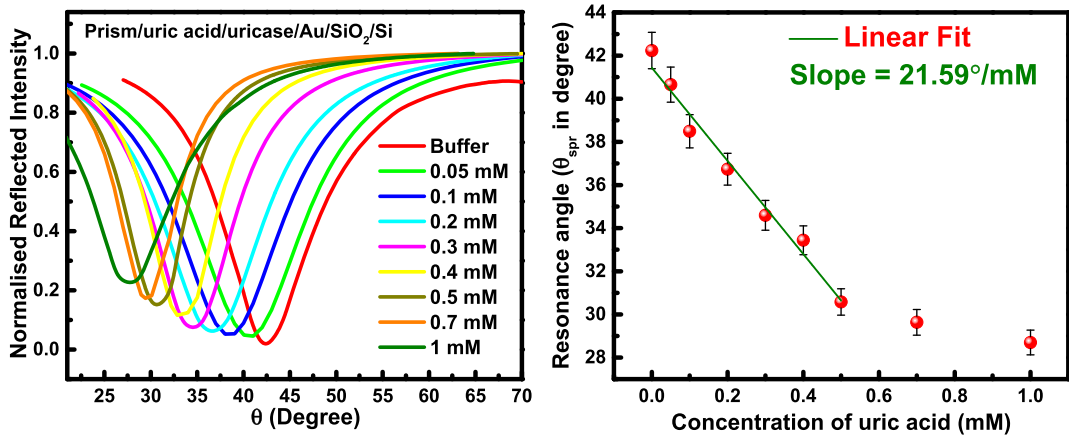

Fig. 4. (a) LRSPR Reflectance curves for the increasing concentrations of Uric acid, (b) Variation in resonance angle with the concentration of uric acid.

$$f_i = \exp(s_2 * (0 + 1j)) \quad (4)$$

$$s_i = 2*k_{zi}*d_i \quad (5)$$

$$r_{345} = (r_{34}+r_{45}*f_4) / (1 + r_{34}*r_{45}*f_4) \quad (6)$$

$$r_{2345} = (r_{23}+r_{345}*f_3) / (1 + r_{23}*r_{345}*f_3) \quad (7)$$

where, ε_i with $i = 1$ to 5 are the dielectric constants of prism, uric acid-uricase, Au, SiO_2 and silicon respectively, λ is wavelength of the incident light, and θ is incident angle of the laser light. The d_2, d_3 and d_4 are thickness of the semi-infinite dielectric media (uric acid-uricase), Au and SiO_2 layer respectively.

As the uric acid concentration is changed, the reflectance value in equation (1) changes as a consequence of variation in refractive index of the dielectric media (uric acid-uricase) in the prism/uric acid–uricase/Au/SiO_2/Si sensor structure. The enzymatic reaction between uric acid (analyte) and uricase enzyme (bio-recognition element) is as follows (Zhao et al., 2009):

$$\text{Uric acid} + O_2 + H_2O \overset{\text{uricase}}{\Leftrightarrow} \text{Allantoin} + CO_2 + H_2O_2$$

As can be seen from Fig. 4(a), the resonance angle, θ_{LRSPR} shifts towards lower angle with increase in the uric acid concentration from 0 mM to 1 mM. This is attributed to the decrease in the refractive index in the vicinity of Uricase/Au interface. As the concentration of uric acid in the PBS solution is increased, higher concentration of Allantoin and H_2O_2 are formed along with the enhanced electron density at the interface of Uricase/Au. Refractive index of uric acid is 1.721 (Ringertz, 1965), whereas the refractive index of the product Allantoin is 1.615

(Gravenmade et al., 2010). Since the refractive index of the product (Allantoin) of the enzymatic reaction (between uricase and uric acid) is lower than uric acid, the effective refractive index of the sensing bulk media decreases. Furthermore, change in the refractive index of sensing medium in contact with matrix (Uricase/Au/SiO_2/Si) on interaction with the biochemical product and uric acid (analyte) is not to be ruled out, that may also lead to a decrease in the effective refractive index. Hence, a decrease in the resonance angle θ_{LRSPR} is observed as a result of the decrease in the refractive index at Uricase/Au interface on increasing the uric acid concentration from 0 mM to 1 mM.

The variation in the Resonance angle with increment in the uric acid concentration is represented in Fig. 4 (b) (Calibration curve). The prepared LRSPR based biosensor exhibits a very good linearity for uric acid in the concentration range from 0.05 to 0.5 mM which lies well within the physiological range for uric acid in a healthy human body (0.16 mM–0.43 mM) (Jindal et al., 2017). With the increasing concentration of target uric acid from 0.05 mM to 0.5 mM, a linear decrease in the value of θ_{LRSPR} from 40.65° to 30.58° can be comprehended from the calibration curve (Fig. 4 (b)). After 0.5 mM, the sensor response tends to saturate at higher concentrations which is well in correspondence to the trends reported in literature (Lu et al., 2012; A W Wark et al., 2005). All the measurements were repeated 5 times for each uric acid concentration and the standard deviation was found to be less than 2%. As estimated from slope of the calibration curve (Fig. 4 (b)), the proposed sensor possesses a high sensitivity of 21.6°/mM towards the uric acid detection. The limit of detection (LOD) of the prepared sensor is found to be 0.02 mM. LOD was evaluated using the equation (Srivastava et al., 2011):

$$LOD = \frac{F \times SD}{b}$$

where, F is proportionality factor, SD is standard deviation corresponding to ordinate intercept of the calibration curve and b is the slope of regression line.

3.3.1. Selectivity and interference studies

To assess the selectivity of the prepared LRSPR biosensor, different analytes of 1 mM concentration such as urea, glucose and ascorbic acid (common interferents present in human body along with uric acid) were kept in contact with the immobilized uricase enzyme in the prism/analyte-uricase/Au/SiO_2/Si configuration and their reflectance curves were recorded. The corresponding variation in the resonance angle (θ_{LRSPR}) is shown in Fig. 5 (a). The prepared sensor structure (prism/analyte-uricase/Au/SiO_2/Si) is highly selective to uric acid, as no

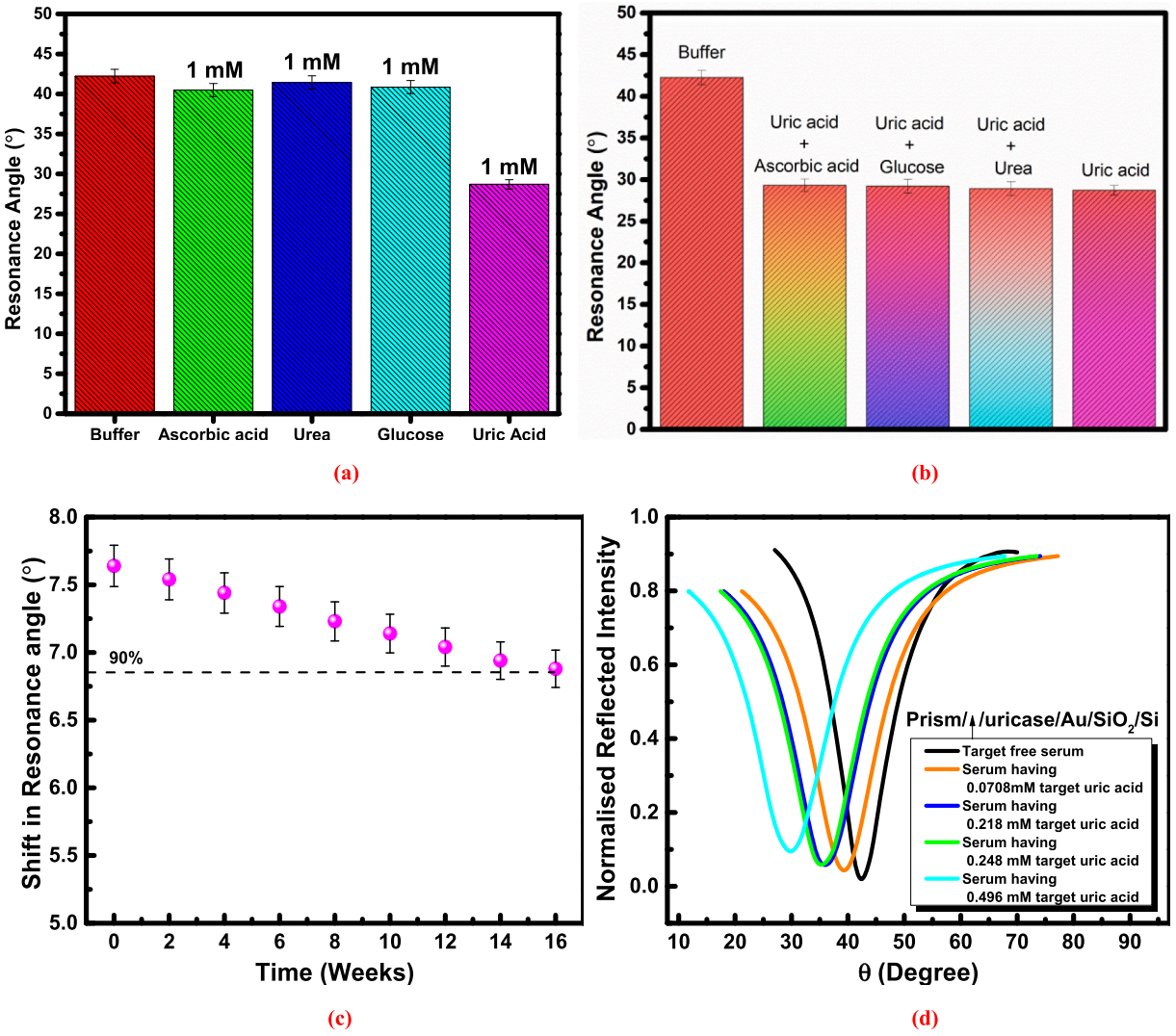

Fig. 5. (a) Selectivity and (b) Interference studies of the Prism/Analyte-Uricase/Au/SiO_2/Si sensor incubation with different analytes e.g. Ascorbic acid, Urea and Glucose, (c) Shelf life analysis of the prepared LRSPR uric acid biosensor, and (d) LRSPR reflectance curves for Prism/uricase/Au/SiO_2/Si structure on incubation with real serum samples having different concentrations of uric acid.

Table 1
Assessment of the prepared LRSPR based uric acid sensor with respect to literature.

Sensor Configuration	Sensing Technique	Performance Characteristics	Reference
Optical fiber/**Ag**/**Si**/Uricase/Uric acid	Optical fiber based SPR (Transmission mode)	LOD = 0.032 mM, Sensitivity = 30 nm/mM	Kant et al. (2016b)
Uric acid imprinted Poly(HEMA-MAC)-Fe^{3+}NPs/**Au**/prism	Molecularly Imprinted SPR using Kretschmann configuration (Angular Interrogation)	LOD = 2.96 μM, response time = 15 min	Göçenoğlu Sarıkaya et al. (2017)
Tapered plastic optical fiber/**ZnO**	Optical fiber based SPR (Transmission mode)	Sensitivity = 0.0025 mV/ppm, LOD = 0.03 mM	Batumalay et al. (2014)
Tapered plastic optical fiber/**Graphene**	Optical fiber based SPR (Transmission mode)	Sensitivity = 0.0021 mV/ppm, LOD = 0.045 mM	(Batumalay et al., 2014b)
Tapered plastic optical fiber/**CNT-polyethylene oxide composite**	Optical fiber based SPR (Transmission mode)	Sensitivity = 0.0023 mV/ppm, LOD = 0.04 mM	Malathy Batumalay et al. (2014a)
Si/**SiO_2**/**Au**/Uricase/uric acid/prism	Long Range Surface Plasmon (LRSPR) using Otto configuration (Angular Interrogation)	LOD = 0.02 mM, Sensitivity = 21.6°/mM	**Present work**

significant shift in the θ_{LRSPR} from reference value is observed in case of different analytes (Urea, Glucose and Ascorbic acid) of 1 mM concentration as compared to the case of uric acid of same concentration (Fig. 5 (a)). Further, the same interfering analytes (1 mM concentration) were mixed with 1 mM concentration of uric acid separately, and the corresponding LRSPR reflectance curves were acquired.

No significant shift is observed in θ_{LRSPR} with high concentration (1 mM) of different analytes (Urea, Glucose and Ascorbic acid) spiked into 1 mM concentration of uric acid (Fig. 5 (b)). Hence, the proposed LRSPR biosensor is highly sensitive to uric acid.

3.3.2. *Shelf life study of the LRSPR biosensor*

To ascertain the shelf life of prepared LRSPR biosensor, the sensing response for a particular concentration (0.3 mM) of uric acid was recorded at fixed time intervals (every week) for a period of 16 weeks. It was found that the prepared LRSPR biosensor is stable for more than 16 weeks as the bioelectrode retains 90% of its activity (Fig. 5 (c)).

3.3.3. *Validation of LRSPR uric acid biosensor*

The LRSPR uric acid biosensor is validated using real serum samples. Initially, the fabricated bioelectrode (prism/uricase/Au/SiO_2/Si) was incubated with target free human serum sample and no shift in the reflectance curve with respect to the reference (bare PBS solution) of prism/uricase/Au/SiO_2/Si system was observed. Subsequently, 4 different concentrations (0.0708 mM, 0.218 mM, 0.248 mM, and 0.496 mM) of uric acid were spiked into the target free human serum samples one by one separately and the corresponding LRSPR reflectance curves were recorded as shown in Fig. 5 (d). The obtained values of θ_{LRSPR} from Fig. 5(d) were compared to the corresponding values in the Calibration curve (Fig. 4 (b)) and are tabulated in Supplementary Table S4. The resonance angle (θ_{LRSPR}) for all measured concentrations of uric acid in real serum samples is found to be in close proximity to the expected values based on the calibration curve. It can be inferred that the fabricated LRSPR biosensor encompasses the ability to detect uric acid even in complex and clinically significant urine serum samples.

3.3.4. *Comparison with reported work on uric acid biosensors*

A number of reports can be found in the literature on electrochemical biosensing of uric acid (Ibupoto et al., 2018; Zhao et al., 2013). Changing ambient conditions such as low humidity and high temperatures tend to dry out the electrochemical sensor's electrolyte thereby decreasing its shelf life and gives poor stability. Mostly, electrochemical biosensors require harmful electron mediating species, which can damage the biocompatible environment. Other challenges associated with electrochemical biosensors include non-specific binding and poor performance with real samples because of the electrode failure or selectivity issue in complex analyte matrix (Putzbach and Ronkainen, 2013). Optical biosensors are favored over conventional electrochemical based biosensors because they are free from any electromagnetic interference and solely depend on change in optical properties thus ensuring high sensitivity with a comparatively high signal to noise ratio. There are only a handful of reports available in literature on optical sensing of uric acid (GRABOWSKA et al., 2008). Kumar et al. reported Ag–nanoparticles (NPs) based optical biosensor for uric acid utilizing radiation grafted polymer support for uricase immobilization (Kumar et al., 2014). They have made use of UV–Visible spectroscopy for detecting uric acid of a fixed concentration. No sensitivity or selectivity studies have been performed on the prepared sensor. Moreover, the synthesis process involved for the sensing module is tedious and expensive. Dual optical detection methods including spectrophotometric and fluorescence were also reported for detection of uric acid in a concentration range from 0.05 mM to 0.3 mM. However, Fluorescence spectroscopy is complex and requires expensive equipments (Kumar et al., 2014). Jin et al. exploited Cadmium telluride (CdTe) Nanoparticles as Fluorescence probes for detecting uric acid in the concentration range from 0 – 6 μM (Jin et al., 2016). CdTe when exposed to human body can damage cell membrane, mitochondria and cell nucleus. Also, Cadmium (Cd) is known to be amongst the most toxic and hazardous elements known (Fthenakis et al., 1999). Amongst the various available optical biosensing techniques, SPR is considered to be quite effective and sensitive (Arghir et al., 2015; Wijaya et al., 2011). Table 1shows the comparison of the characteristics of the prepared LRSPR based biosensor with the reported SPR based uric acid biosensors. Kant et al. reported an optical fiber based SPR sensor utilizing Si as sensing layer for detecting uric acid in the concentration range from 0.1 mM to 0.9 mM. LOD achieved with their sensor is 0.032 mM which is relatively higher (Kant et al., 2016). Molecular imprinted SPR sensing technique in Kretschmann configuration is utilized by Sarikaya et al. for detecting uric acid in concentration range (2.97 μM–0.24 mM) (Göçenoğlu Sarıkaya et al., 2017). They made use of the Uric acid (UA) embossed poly (HEMA-MAC)-Fe3+ nanoparticles for the sensing purpose. However, the process involved in the preparation of the sensor is complex and tedious (Göçenoğlu Sarıkaya et al., 2017). Batumalay et al. reported uric acid sensors (concentration range 0.57 mM–2.88 mM) based on ZnO coated tapered optical fiber, Graphene and single wall CNT (SWCNT) polyethylene oxide composite (M. Batumalay et al., 2014; Malathy Batumalay et al., 2014b, 2014a). The LOD achieved by the sensors, with ZnO, Graphene and single wall CNT polyethylene oxide composite, sensing layers are 0.03 mM, 0.045 mM and 0.04 mM respectively (M. Batumalay et al., 2014; Malathy Batumalay et al., 2014a, 2014b). However no selectivity studies were performed to assess the performance of the sensors. These shortcomings are efficiently overcome by the prepared LRSPR based uric acid biosensor (Table 1). There are no reports available on LRSPR based uric acid biosensor, to the best of our knowledge. The prepared LRSPR biosensor is encapsulated with ease of fabrication, handling, high sensitivity and selectivity. Also the dielectric layer utilized in the LRSPR biosensor i.e. SiO_2 (with tunable refractive index) is eco-friendly and easy to deposit. The major benefits of the fabricated LRSPR based biosensor are high precision as compared to conventional SPR based biosensors and label-free concept.

4. Conclusions

In the present study, SiO_2 nanostructured film deposited at an oblique angle of 80° and deposition pressure of 30 mTorr using oblique angle assisted RF sputtering technique exhibits the lowest refractive index of about 1.33 and was employed as dielectric layer in the LRSPR biosensor structure Si/SiO_2/Au/uricase-uric acid/prism, for detecting uric acid in the concentration range from 0.05 mM to 1 mM. The prepared LRSPR sensor demonstrated high sensitivity of 21.6°/mM towards uric acid and LOD of 0.02 mM. Selectivity of the LRSPR biosensor was investigated by assessing the response towards the different interfering analytes. The comprehended results signify the ability of Si/SiO_2/Au/uricase-uric acid/prism LRSPR sensor to efficiently and precisely detect uric acid over an extensive concentration range. The prepared LRSPR sensor is also validated by testing real human serum samples. The obtained results are encouraging towards the development of highly sensitive and specific LRSPR based biosensors utilizing SiO_2 as the dielectric sensing layer.

CRediT authorship contribution statement

Surbhi Jain: Conceptualization, Methodology, Writing - original draft. **Ayushi Paliwal:** Writing - review & editing, Visualization. **Vinay Gupta:** Writing - review & editing, Conceptualization, Supervision, Resources. **Monika Tomar:** Writing - review & editing, Conceptualization, Supervision, Resources.

Declaration of competing interest

The authors declare that they have no known competing financial interests or personal relationships that could have appeared to influence the work reported in this paper.

Acknowledgment

The authors are thankful to the Department of Science and Technology (DST), Government of India and Department of Physics and Astrophysics, University of Delhi for all the facilities and financial support. One of the authors SJ is grateful to University Grants Commission (UGC) for the research fellowship.

Appendix A. Supplementary data

Supplementary data to this article can be found online at https://doi.org/10.1016/j.bios.2020.112508.

References

Ahuja, D., Parande, D., 2012. Optical sensors and their applications. Journal of Scientific Research and Reviews.

Arghir, I., Spasic, D., Verlinden, B.E., Delport, F., Lammertyn, J., 2015. Improved surface plasmon resonance biosensing using silanized optical fibers. Sensor. Actuator. B Chem. 216, 518–526. https://doi.org/10.1016/j.snb.2015.04.069.

Arora, S., Kaur, T., Kaur, A., Singh, A.P., 2014. Glycine aggravates ischemia reperfusion-induced acute kidney injury through N-methyl-D-aspartate receptor activation in rats. Mol. Cell. Biochem. 393, 123–131. https://doi.org/10.1007/s11010-014-2052-0.

Astrova, E.V., Tolmachev, V.A., 2000. Effective refractive index and composition of oxidized porous silicon films. Mater. Sci. Eng. B 69–70, 142–148. https://doi.org/10.1016/S0921-5107(99)00236-6.

Batumalay, M., Harith, Z., Rafaie, H.A., Ahmad, F., Khasanah, M., Harun, S.W., Nor, R. M., Ahmad, H., 2014. Tapered plastic optical fiber coated with ZnO nanostructures for the measurement of uric acid concentrations and changes in relative humidity. Sensors Actuators A Phys 210, 190–196. https://doi.org/10.1016/j.sna.2014.01.035.

Batumalay, Malathy, Ahmad, F., Lokman, A., Jasim, A.A., Wadi Harun, S., Ahmad, H., 2014a. Tapered plastic optical fiber coated with single wall carbon nanotubes polyethylene oxide composite for measurement of uric acid concentration. Sens. Rev. 34, 75–79. https://doi.org/10.1108/SR-09-2012-699.

Batumalay, Malathy, Harun, S.W., Ahmad, F., Nor, R.M., Zulkepely, N.R., Ahmad, H., 2014b. Tapered plastic optical fiber coated with Graphene for uric acid detection. IEEE Sensor. J. 14, 1704–1709. https://doi.org/10.1109/JSEN.2014.2302900.

Béland, P., Krupin, O., Berini, P., 2015. Selective detection of bacteria in urine with a long-range surface plasmon waveguide biosensor. Biomed. Optic Express 6, 2908. https://doi.org/10.1364/BOE.6.002908.

Berini, P., 2009. Long-range surface plasmon polaritons. Adv. Optic Photon 1, 484. https://doi.org/10.1364/AOP.1.000484.

Berini, P., Charbonneau, R., Lahoud, N., 2007. Long-range surface plasmons on ultrathin membranes. Nano Lett. 7, 1376–1380. https://doi.org/10.1021/nl070464w.

Colette McDonagh, Conor, S., Burke, MacCraith*, Brian D., 2008. Optical Chemical Sensors. https://doi.org/10.1021/CR068102G.

Damborsky, P., vitel, J., Katrlik, J., 2016. Optical biosensors. Essays Biochem. 60, 91–100. https://doi.org/10.1042/EBC20150010.

Deshmukh, S.C., Aydil, E.S., 1994. Low-temperature plasma enhanced chemical vapor deposition of SiO2. Appl. Phys. Lett. 65, 3185–3187. https://doi.org/10.1063/1.112475.

Dewan, S., Paliwal, A., Tomar, M., Kapoor, A.K., Tandon, R.P., Gupta, V., 2018. Surface plasmon resonance aided analysis of quantum wells for photonic device applications. Mater. Des. 150, 94–103. https://doi.org/10.1016/j.matdes.2018.04.010.

Dostálek, J., Kasry, A., Knoll, W., 2007. Long range surface plasmons for observation of biomolecular binding events at metallic surfaces. Plasmonics 2, 97–106. https://doi.org/10.1007/s11468-007-9037-8.

Fthenakis, V.M., Morris, S.C., Moskowitz, P.D., Morgan, D.L., 1999. Toxicity of cadmium telluride, copper indium diselenide, and copper gallium diselenide. Prog. Photovoltaics Res. Appl. 7, 489–497. https://doi.org/10.1002/(SICI)1099-159X(199911/12)7:6<489::AID-PIP287>3.0.CO;2-N.

Göçenoğlu Sarıkaya, A., Osman, B., Çam, T., Denizli, A., 2017. Molecularly imprinted surface plasmon resonance (SPR) sensor for uric acid determination. Sensor. Actuator. B Chem. 251, 763–772. https://doi.org/10.1016/j.snb.2017.05.079.

Grabowska, I., Chudy, M., Dybko, A., Brzozka, Z., 2008. Uric acid determination in a miniaturized flow system with dual optical detection. Sensor. Actuator. B Chem. 130, 508–513. https://doi.org/10.1016/j.snb.2007.09.051.

Gravenmade, E.J., Vogels, G.D., van Pelt, C., 2010. Preparation, properties and absolute configuration of (-)-allantoin. Recl. des Trav. Chim. des Pays-Bas 88, 929–939. https://doi.org/10.1002/recl.19690880806.

Herrasti, Z., Martínez, F., Baldrich, E., 2016. Detection of uric acid at reversibly nanostructured thin-film microelectrodes. Sensor. Actuator. B Chem. 234, 667–673. https://doi.org/10.1016/j.snb.2016.05.018.

Ibupoto, Z.H., Tahira, A., Raza, H., Ali, G., Khand, A.A., Jilani, N.S., Mallah, A.B., Yu, C., Willander, M., 2018. Synthesis of heart/dumbbell-like CuO functional nanostructures for the development of uric acid biosensor. Materials 11, 1–13. https://doi.org/10.3390/ma11081378.

Jin, D., Seo, M.-H., Huy, B.T., Pham, Q.-T., Conte, M.L., Thangadurai, D., Lee, Y.-I., 2016. Quantitative determination of uric acid using CdTe nanoparticles as fluorescence probes. Biosens. Bioelectron. 77, 359–365. https://doi.org/10.1016/j.bios.2015.09.057.

Jindal, K., Tomar, M., Gupta, V., 2013. Nitrogen-doped zinc oxide thin films biosensor for determination of uric acid. Analyst 138, 4353. https://doi.org/10.1039/c3an36695b.

Jindal, K., Tomar, M., Gupta, V., 2017. A novel low-powered uric acid biosensor based on arrayed p-n junction heterostructures of ZnO thin film and CuO microclusters. Sensor. Actuator. B Chem. 253, 566–575. https://doi.org/10.1016/j.snb.2017.06.146.

Kant, R., Tabassum, R., Gupta, B.D., 2016. Fiber optic SPR-based uric acid biosensor using uricase entrapped polyacrylamide gel. IEEE Photon. Technol. Lett. 28, 2050–2053. https://doi.org/10.1109/LPT.2016.2571722.

Kasry, A., Knoll, W., 2006. Long range surface plasmon fluorescence spectroscopy. Cit. Appl. Phys. Lett. J. Appl. Phys. Appl. Phys. Lett. 891, 101106–107149. https://doi.org/10.1063/1.2345594.

Krupin, O., Wang, C., Berini, P., 2015. Detection of leukemia markers using long-range surface plasmon waveguides functionalized with Protein G. Lab Chip 15, 4156–4165. https://doi.org/10.1039/C5LC00940E.

Kumar, V., Misra, N., Paul, J., Dhanawade, B.R., Varshney, L., 2014. Uricase-immobilization on radiation grafted polymer support for detection of uric acid using Ag-nanoparticle based optical biosensor. Polymer (Guildf). 55, 2652–2660. https://doi.org/10.1016/j.polymer.2014.04.012.

Lu, X., Zheng, H., Li, X.-Q., Yuan, X.-X., Li, H., Deng, L.-G., Zhang, H., Wang, W.-Z., Yang, G.-S., Meng, M., Xi, R.-M., Aboul-Enein, H.Y., 2012. Detection of ractopamine residues in pork by surface plasmon resonance-based biosensor inhibition immunoassay. Food Chem. 130, 1061–1065. https://doi.org/10.1016/J.FOODCHEM.2011.07.133.

Manera, M.G., Rella, R., 2013. Improved gas sensing performances in SPR sensors by transducers activation. Sensor. Actuator. B Chem. 179, 175–186. https://doi.org/10.1016/J.SNB.2012.10.028.

Matsuoka, J., Kitamura, N., Fujinaga, S., Kitaoka, T., Yamashita, H., 1991. Temperature dependence of refractive index of SiO2 glass. J. Non-Cryst. Solids 135, 86–89. https://doi.org/10.1016/0022-3093(91)90447-E.

Méjard, R., Dostálek, J., Huang, C.J., Griesser, H., Thierry, B., 2013. Tuneable and robust long range surface plasmon resonance for biosensing applications. Opt. Mater. (Amst). 35, 2507–2513. https://doi.org/10.1016/j.optmat.2013.07.011.

Nooke, A., Beck, U., Hertwig, A., Krause, A., Krüger, H., Lohse, V., Negendank, D., Steinbach, J., 2010. On the application of gold based SPR sensors for the detection of hazardous gases. Sensor. Actuator. B Chem. 149, 194–198. https://doi.org/10.1016/J.SNB.2010.05.061.

Paliwal, A., Tomar, M., Gupta, V., 2014. Complex dielectric constant of various biomolecules as a function of wavelength using surface plasmon resonance. J. Appl. Phys. 116 https://doi.org/10.1063/1.4890027.

Paliwal, A., Tomar, M., Gupta, V., 2018. Refractive index sensor using long-range surface plasmon resonance with prism coupler. Plasmonics 1–7. https://doi.org/10.1007/s11468-018-0814-3.

Putzbach, W., Ronkainen, N., 2013. Immobilization techniques in the fabrication of nanomaterial-based electrochemical biosensors: a review. Sensors 13, 4811–4840. https://doi.org/10.3390/s130404811.

Ringertz, H., 1965. Optical and crystallographic data of uric acid and its dihydrate. Acta Crystallogr. 19, 286–287. https://doi.org/10.1107/s0365110x65003298.

Ryu, S.R., Noda, I., Jung, Y.M., 2010. What is the origin of positional fluctuation of spectral features: true frequency shift or relative intensity changes of two overlapped bands? Appl. Spectrosc. 64, 1017–1021. https://doi.org/10.1366/000370210792434396.

Slavík, R., Homola, J., 2007. Ultrahigh resolution long range surface plasmon-based sensor. Sensor. Actuator. B Chem. 123, 10–12. https://doi.org/10.1016/j.snb.2006.08.020.

Srivastava, S.K., Verma, R., Gupta, B.D., 2011. Surface plasmon resonance based fiber optic sensor for the detection of low water content in ethanol. Sensor. Actuator. B Chem. 153, 194–198. https://doi.org/10.1016/j.snb.2010.10.038.

Wang, Y., Dostálek, J., Knoll, W., 2009. Long range surface plasmon-enhanced fluorescence spectroscopy for the detection of aflatoxin M1 in milk. Biosens. Bioelectron. 24, 2264–2267. https://doi.org/10.1016/j.bios.2008.10.029.

Wark, A.W., Lee, H.J., Corn, R.M., 2005. Long-range surface plasmon resonance imaging for bioaffinity sensors. Anal. Chem. 77, 3904–3907. https://doi.org/10.1021/ac050402v.

Wijaya, E., Lenaerts, C., Maricot, S., Hastanin, J., Habraken, S., Vilcot, J.-P., Boukherroub, R., Szunerits, S., 2011. Surface plasmon resonance-based biosensors: from the development of different SPR structures to novel surface functionalization strategies. Curr. Opin. Solid State Mater. Sci. 15, 208–224. https://doi.org/10.1016/J.COSSMS.2011.05.001.

Xi, J.Q., Schubert, M.F., Kim, J.K., Schubert, E.F., Chen, M., Lin, S.Y., Liu, W., Smart, J. A., 2007. Optical thin-film materials with low refractive index for broadband elimination of Fresnel reflection. Nat. Photon. 1, 176–179. https://doi.org/10.1038/nphoton.2007.26.

Yuan, Y., Dai, Y., 2014. A revised LRSPR sensor with sharp reflection spectrum. Sensors (Switzerland) 14, 16664–16671. https://doi.org/10.3390/s140916664.

Zhao, Y., Yang, X., Lu, W., Liao, H., Liao, F., 2009. Uricase based methods for determination of uric acid in serum. Microchim. Acta. https://doi.org/10.1007/s00604-008-0044-z.

Zhao, Y., Yan, X., Kang, Z., Lin, P., Fang, X., Lei, Y., Ma, S., Zhang, Y., 2013. Highly sensitive uric acid biosensor based on individual zinc oxide micro/nanowires. Microchim. Acta 180, 759–766. https://doi.org/10.1007/s00604-013-0981-z.